CMT—Conductivity-Modulated Transistor

Bogdan M. Wilamowski, *Senior Member, IEEE*, and Thad J. Englert, *Member, IEEE*

Abstract—**The characteristics of a conductivity-modulated transistor, which is able to control ac current are presented. Measured characteristics of a fabricated device are shown and compared with calculated characteristics. Calculations are based on a physical, one-dimensional analytical model which has been, in part, derived from numerical analysis of the device. The proposed model gives relatively good qualitative agreement between calculated and measured characteristics. Potential applications of the device are discussed.**

I. Introduction

THE UNIJUNCTION transistor is a well-known device which uses the effect of conductivity modulation for its operation [1]–[3]. This device bears the name "transistor" probably because it is a three-terminal device; however, it has limited application since it exhibits mainly negative resistance. It does not have current or voltage gain, cannot be used as an amplifier, and is used mainly as a latch where the advantage of the negative input resistance can be taken. Recently, the Unijunction Transistor lost importance because in most applications it can be substituted by an integrated circuit which consists of two bipolar transistors and one or two resistors [5]. This integrated circuit, commonly known as Programmable Unijunction Transistor, is less expensive and has much better parameters than the original Unijunction Transistor, these parameters being modifiable by external resistors.

The proposed CMT is also a single p-n junction device but operates as a transistor with current and voltage gains and, what is more important, can be used for controlling ac currents of both polarizations without the necessity of adding dc biasing as in all other transistor amplifiers. In the case of n-type bases and p-type emitter (refer to Fig. 1), if base B_1 is grounded, the controlling current injected through the emitter controls even large current flowing between bases B_2 and B_1, no matter whether B_1 has positive or negative biasing.

The negative resistance seen from the emitter, which is the main advantage of the unijunction transistor in this case, is considered as a parasitic effect and is eliminated by proper device construction. In this paper we present experiment, numerical analysis, and an analytical model which describes the qualitative behavior of the CMT.

Manuscript received October 22, 1990; revised December 16, 1991. The review of this paper was arranged by Associate Editor T. P. Chow.

The authors are with the Department of Electrical Engineering, University of Wyoming, Laramie, WY 82071-3295.

IEEE Log Number 9202944.

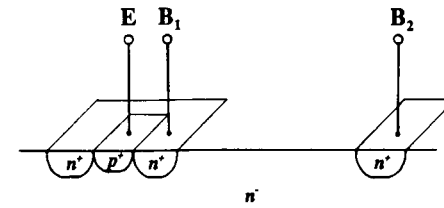

Fig. 1. Cross section of the Conductivity Modulated Transistor.

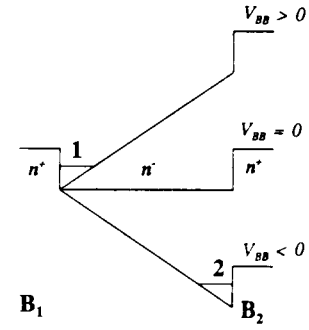

Fig. 2. Shapes of the potential distributions along the device for positive and negative polarization of base B_2. Note potential barriers controlling device current in region 1 for positive voltage on B_2 and region 2 for negative voltage on B_2.

II. Device Description and Operating Principle

The device cross section is shown in Fig. 1 and potential distributions for positive and negative biasing can be seen in Fig. 2. Holes injected into the n^- region will be swept toward the lowest potential by the electrical field within the device. With positive biasing on B_2 hole accumulation will occur near B_1 while with negative biasing on B_2 hole accumulation will occur near B_2. In either biasing configuration holes are trapped by the potential well and the number of accumulated holes in the vicinity of the potential barrier will depend upon the local recombination rate. The voltage drop across a region of hole accumulation is quite small due to the effect of conductivity modulation. In this manner, the device operation is relatively independent of the electric polarity between B_1 and B_2.

The device structure shown in Fig. 1 was fabricated. Lightly doped n-type silicon, with ⟨111⟩ orientation and very high resistivity (600 Ω · cm), was used as the substrate. The n^+ bases were formed by a phosphor diffused layer with 5-Ω sheet resistance and 2.2-μm depth. The emitter was formed by a boron diffusion layer with a sheet resistance of approximately 100 Ω. Electrical contact was provided by an aluminum layer evaporated in an electron-beam system and annealed at 420°C in forming gas (15%

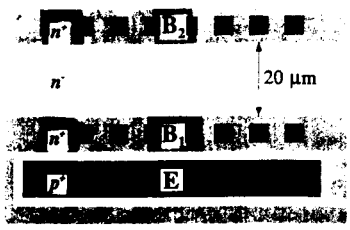

Fig. 3. Topology of the fabricated CMT structure (metallization layer is not shown).

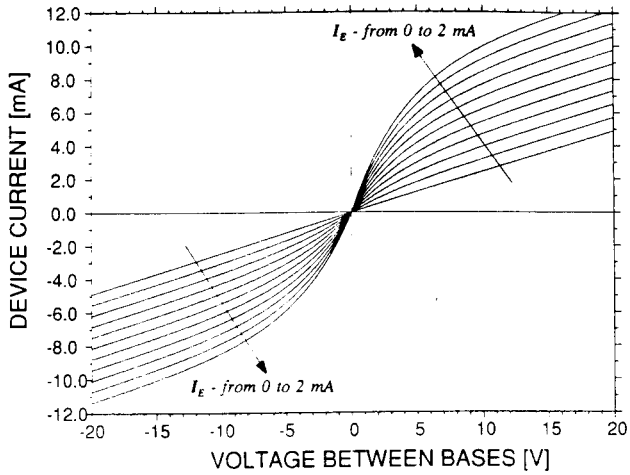

Fig. 4. Measured current–voltage characteristics between bases B_1 and B_2 with the emitter current I_E as parameter varied from 0 to 2 mA in increments of 0.2 mA.

H_2) for 30 min. A top view of the structure layout without metallization is shown in Fig. 3.

The measured device characteristics are shown in Fig. 4. It is worthwhile to notice that current gain is larger than 1 (approximately 4). The device has the unique characteristics of allowing for proper operation for both polarities of B_1-B_2 base voltages while the controlling emitter current direction remains unchanged. Also it should be noted that in the vicinity of zero biasing, the device has extremely linear characteristics. In fact, it behaves as a variable resistor controlled by current injected by the emitter.

III. Numerical Analysis

In order to fully understand the device operation, numerical analyses were performed. Despite the fact that the device was approximated by a one-dimensional structure, the numerical algorithm dealt with all five important differential equations for semiconductor theory: Poisson's equation, two transport equations, and two continuity equations. The Schockley-Read-Hall (SRH) recombination mechanism model was used in computations.

The solution obtained by the algorithm is quite general. In order to otain a true picture of the physical phenomena no frequently used assumptions such as charge neutrality or dominance of one type of carrier, were taken. A detailed description of the numerical algorithm is given in [6] and will not be repeated here. Only boundary conditions and a one-dimensional approximation of the three-dimensional case will be discussed in detail. It would have been relatively easy to incorporate some secondary effects such as mobility dependence on impurity concentration or on the electrical field, but these were neglected on purpose to eliminate extra "noise."

Because dimensions were artificially reduced from the real three-dimensional structure to the one-dimensional analysis, quantitative agreement may not be expected; however, more important at this stage is quality information. Since quantitative information was not vital, constant values of mobility were assumed. Errors generated by this assumption are not very significant since the electrical field does not reach excessive values.

The following simplifying assumptions were taken in order to reduce dimensions from three to one:

1) The current due to injected holes (emitter current) is taken to be the recombination current, $J_R = qR\Delta x$, assuming all injected holes recombine. This approach neglects another component of emitter current, namely, the current of injected electrons from the n^- region to the emitter. Such injected electron current will be negligibly small compared to the hole current.

2) Hole concentration was computed in such a way as to meet the following two conditions:

a) The total recombination current was equal to I_E, and was proportional to the total number of accumulated holes in the vicinity of a potential barrier.
b) With the existing potential distribution the hole current along the device was assumed to be zero. This condition gives the distribution of the accumulated holes.

Although the algorithm used was fast and efficient, the foregoing requirements created some calculational problems. These problems are attributed to the calculation of hole distributions by using the potential distribution coupled with the requirement that the number of accumulated holes be consistent with the recombination current (emitter current). Of course, the computed hole distribution affects the potential distribution therefore requiring many iterations in order to achieve convergency. With the above requirements, the computing time was almost two orders of magnitude longer than in the case when no hole injection was assumed.

The first case investigated was for no hole injection. Base B_1 was grounded and the voltage on base B_2 was allowed to range from -10 to $+10$ V. Fig. 5 shows the electron concentration distribution. Figs. 6 and 7 show the potential distribution across the device. Fig. 7 is a scaled-up version of Fig. 6 in order that the potential barrier shape, as a function of voltage, can be clearly seen. One can observe that current in the device is controlled by two potential barriers which are dependent on the biasing voltages between bases B_1 and B_2. For positive voltage on B_2, the barrier near base B_1 becomes important, for negative voltages on B_2, the barrier near B_2 controls the current flow.

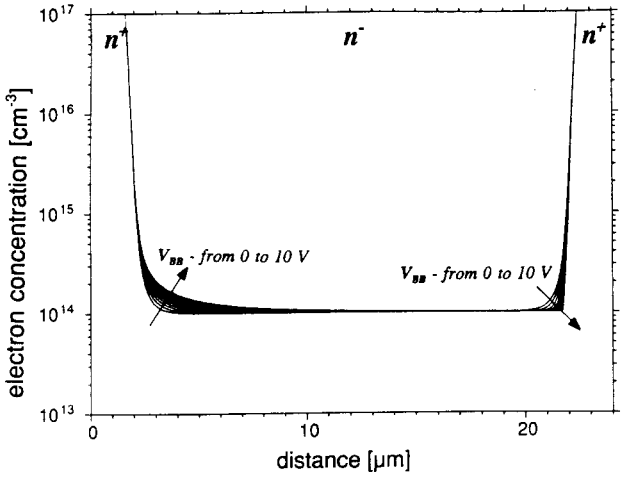

Fig. 5. Results of numerical simulation of the CMT showing the calculated electron distributions along the device for voltages on B_2 varying from 0 to 10 V and no hole injection. Note Gaussian distributions of n^+ bases B_1 and B_2 which penetrate toward the n^- region approximately 2 μm on each side.

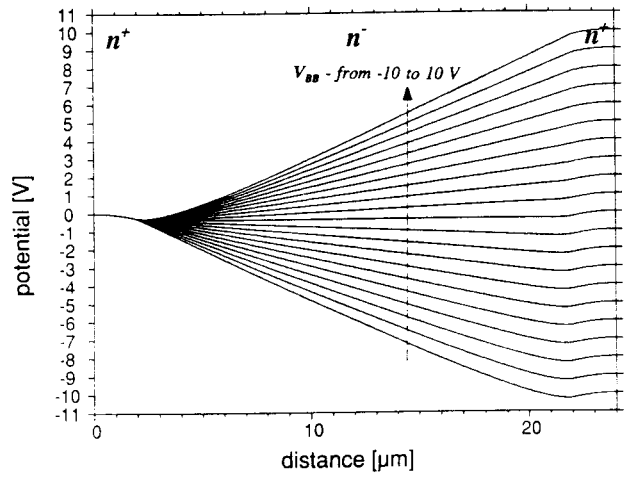

Fig. 6. Results of numerical simulation of the CMT showing the calculated potential distributions along the device for voltages on B_2 varying from 0 to 10 V in 1-V increments and no hole injection.

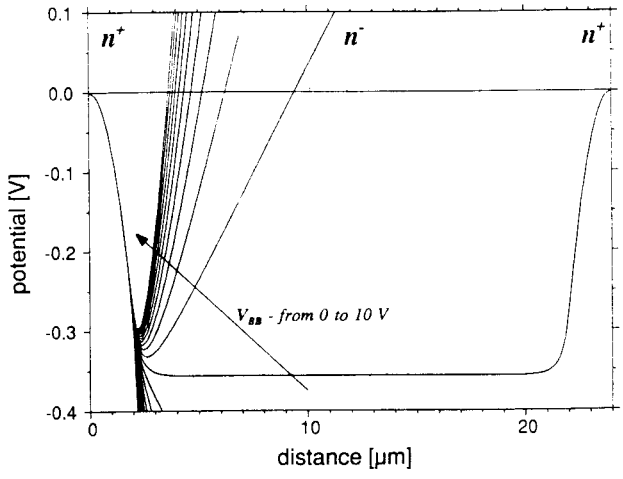

Fig. 7. Scaled up version of Fig. 6 showing potential barrier shapes with no hole injection.

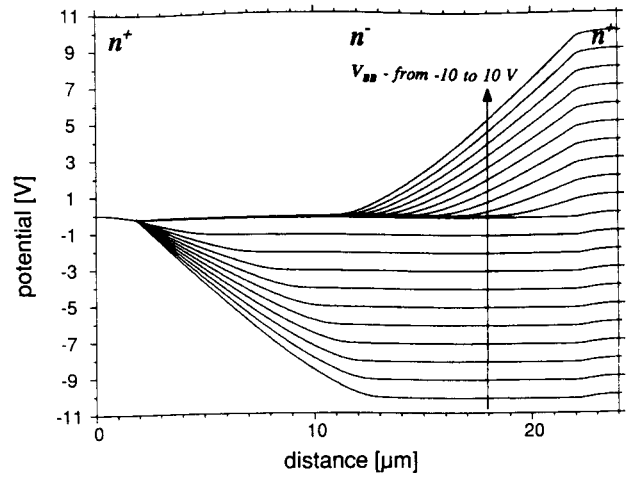

Fig. 8. Results of numerical simulation along the CMT showing the calculated potential distributions along the device for voltages on B_2 varying from 0 to 10 V in 1-V increments and with a hole injection current I_E = 10 A/cm.

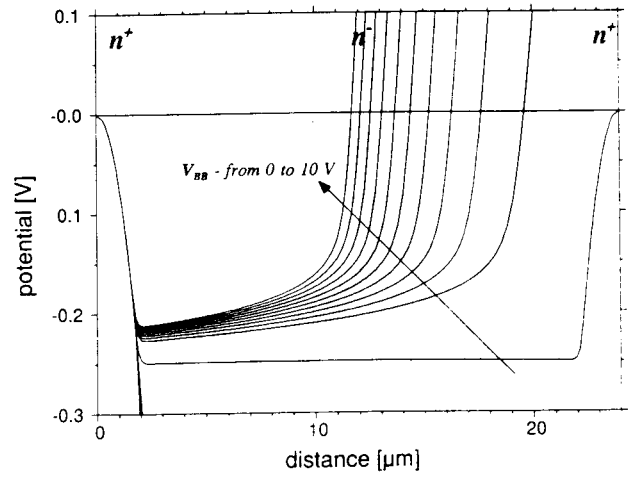

Fig. 9. Scaled up version of Fig. 8 showing potential barrier shapes in the presence of hole injection.

Figs. 8 and 9 show the potential distributions for the case when holes are injected into the n^- region. It can be seen that there is a very significant variation in the potential distribution, especially in barrier width, in comparison with Figs. 6 and 7. Fig. 10 shows the electron distributions, for voltages between bases varying from -10 to $+10$ V, in the presence of hole injection. Note that for positive and negative biasing voltages electron distributions are symmetrical about some point along the distance axis. The same kind of symmetry can also be observed in the electrical field, charge, hole concentration, and recombination rate distributions. Therefore, to obtain a clear picture the following results of numerical computation will be shown only for the case of positive biasing between bases B_2 and B_1. Figs. 11–13 show the hole, electron, and charge distributions, respectively. It is of interest to observe that in the vicinity of the barrier, the charge neutrality condition is valid. This is to be expected since the charge of injected holes is compensated for by a charge of mobile electrons.

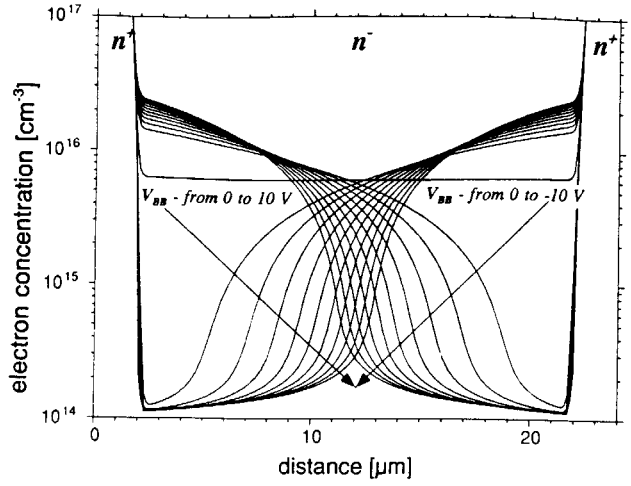

Fig. 10. Results of numerical simulation of the CMT showing the electron distribution in the presence of hole injection I_E = 10 A/cm for voltages on B_2 varying from −10 to 10 V in 1-V increments. Note the symmetry about the 12-μm position.

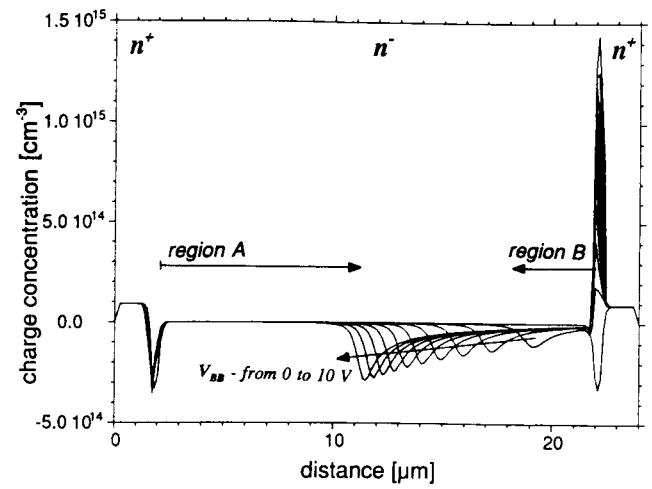

Fig. 13. Charge distributions calculated from numerical simulations if the CMT with the same conditions as in Figs. 11 and 12. Charge neutrality is clearly shown in region *A*.

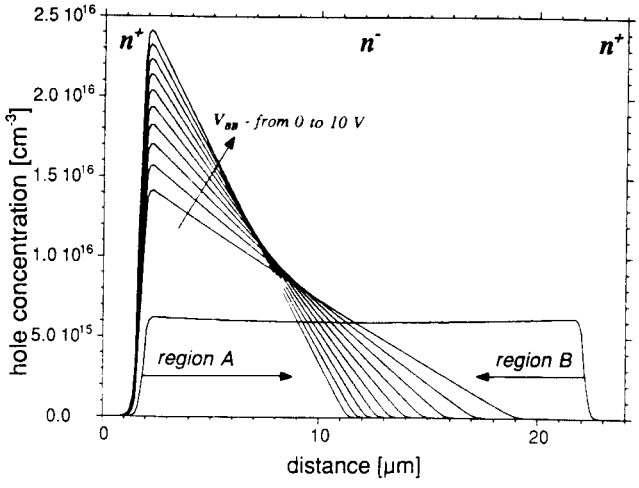

Fig. 11. Hole distribution calculated from numerical simulation of the CMT for voltage on B_2 varying from 0 to 10 V in 1-V increments with hole injection current I_E = 10 A/cm. Note linearity in region *A* and zero concentration in region *B*.

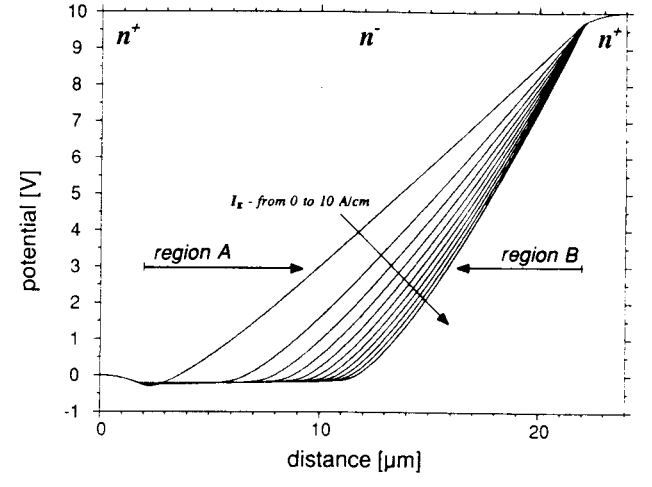

Fig. 14. Simulation results for the CMT showing potential distribution with the emitter current varying from 0 to 10 A/cm in 1-A/cm increments with fixed 10 V at B_2.

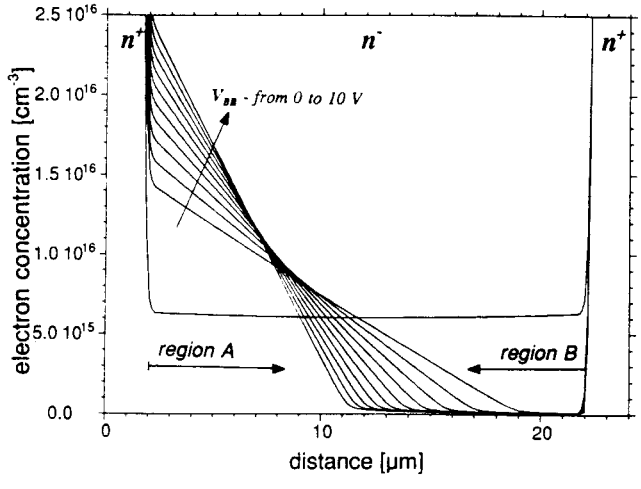

Fig. 12. Electron distribution calculated from numerical simulation of the CMT for voltage on B_2 varying from 0 to 10 V in 1-V increments with hole injection current I_E = 10 A/cm. Note linearity in region *A* as well as the same magnitude as holes in region *A*.

In order to observe the effect of hole injection on the device phenomena another set of potential, hole, and electron distributions is shown in Figs. 14–16. In this case the voltage between B_1 and B_2 is kept constant (V_{BB} = 10 V) and the number of injected holes is varied.

IV. Analytical Approach

A general analytical analysis of the conductivity-modulated transistor is very difficult. Let us, therefore, consider two simple cases: one for very large voltages applied between bases and the other for very small voltages applied between bases.

A. Case 1—Large Voltages Applied Between Bases

Analyzing the results of the numerical simulation (see Figs. 8, 9, 11–13) the following may be concluded:

1) The lightly doped n^- region can be divided into two regions, region *A* close to the base with a lower potential where the electrical field is negligibly small, and region

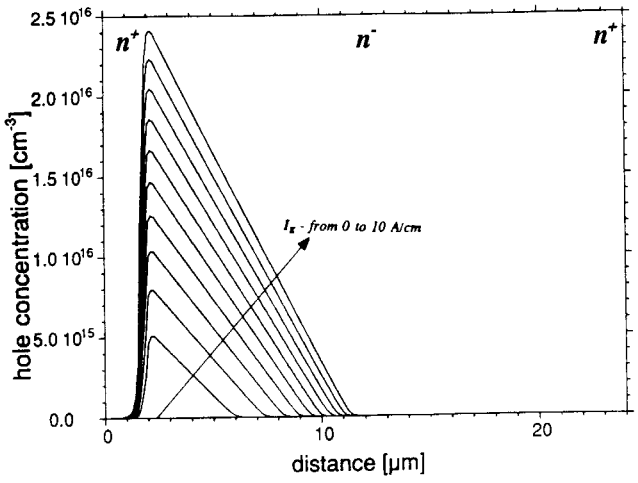

Fig. 15. Simulation results for the CMT showing hole distribution with the emitter current varying from 0 to 10 A/cm in 1-A/cm increments with fixed 10 V at B_2.

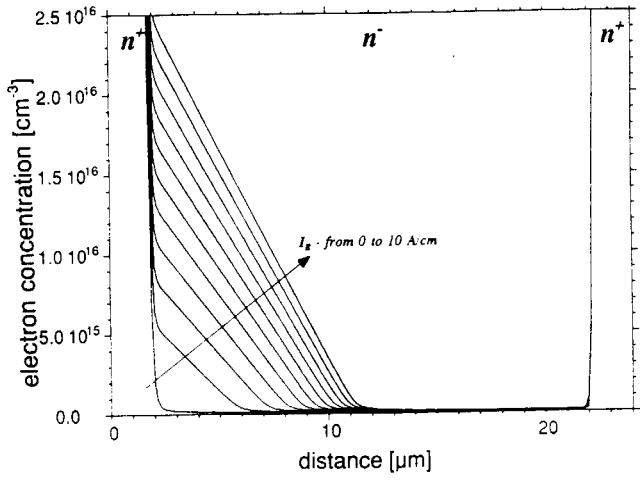

Fig. 16. Simulation results for the CMT showing electron distribution with the emitter current varying from 0 to 10 A/cm in 1-A/cm increments with fixed 10 V at B_2.

B close to the base with a higher potential where almost all the voltage drop occurs (see Figs. 8 and 9).

2) In region A the total charge is negligibly small and the charge neutrality condition is satisfied (see Fig. 13) yielding

$$n = p + N_D = p + n_B. \tag{1}$$

Here $n_B = N_D$ is the electron background concentration in the n^- region. Since in the n^- region N_D = const. or negligibly small based on (1), one can also write

$$\frac{dn}{dx} = \frac{dp}{dx}. \tag{2}$$

3) Carrier distributions are nearly linear in region A (see Figs. 11, 12).

4) In region B the hole concentration is negligibly small and electrons are the only carriers to be considered. In this region drift is the dominant transport mechanism.

Considering region A and assuming that hole current is negligibly small using the Einstein relation $D_p = V_T \mu_p$ (where $V_T = kT/q$) we may write

$$J_p = q\mu_p p\left(-\frac{V_T}{p}\frac{dp}{dx} - \frac{d\psi}{dx}\right) = 0 \tag{3}$$

or

$$\frac{d\psi}{dx} = -\frac{V_T}{p}\frac{dp}{dx}. \tag{4}$$

With the electrical field as above the electron current is given by

$$J_n = qD_n\frac{dn}{dx} + q\mu_n V_T\frac{n}{p}\frac{dp}{dx} = 2qD_n\frac{dp}{dx}. \tag{5}$$

Note that in region A electron and hole concentrations are much larger than the impurity concentration (see Figs. 11, 12) and there the electron and hole concentrations are nearly equal $n \approx p$. Because of the linear electron and hole distributions in region A (see Figs. 11, 12) one can also write (5) in a form

$$J_n = -2qD_n\frac{p_{\max}}{w_A} \tag{6}$$

where $p_{\max}$ is the peak hole concentration in region A and w_A is the length of region A.

In region B drift is the dominant mechanism and current can be expressed by

$$J_n = -q\mu_n n_B\frac{d\psi}{dx} = -q\mu_n n_B\frac{V_B}{w_B} \tag{7}$$

where V_B is the voltage drop on region B (Since the voltage drop on region A is negligibly small the voltage on region B is equal to the entire voltage applied between device bases.) and w_B is the length of region B.

Using (6) and (7) the total length of the device w_T can be written as

$$w_T = w_A + w_B = -\frac{q\mu_n}{J_n}(2V_T p_{\max} + n_B V_{BB}). \tag{8}$$

Device current can then be expressed as

$$J_n = -2qD_n\frac{p_{\max}}{w_T} - q\mu_n n_B\frac{V_{BB}}{w_T}. \tag{9}$$

Note that $p_{\max}$ represents the amount of injected holes and $p_{\max}$ is somewhat proportional to the emitter current I_E.

B. Case 2—Small Voltages Applied Between Bases

In the case of small applied voltages region B disappears and in region A using (2), (4), and (5), one can write

$$J_n = -q\mu_n\frac{d\psi}{dx}(2p + n_B) \approx -q\mu_n(2p_{\text{avg}} + n_B)\frac{V_{BB}}{w_T} \tag{10}$$

where the average hole concentration is given by

$$p_{\text{avg}} = \frac{p_{\max}}{2}. \tag{11}$$

Combining (10) and (11) the device current for small voltages can be expressed by

$$J_n = -q\mu_n \frac{V_{BB}}{w_T}(p_{\max} + n_B). \tag{12}$$

V. Transistor Model

Equations (9) and (12), for small and large voltages applied between bases, can be matched together by the general equation

$$J_n = -\frac{q\mu_n p_{\max} V_{BB}}{w_T}\left[1 - \exp\left(-\frac{2V_T}{V_{BB}}\right)\right] - \frac{q\mu_n n_B V_{BB}}{w_T}. \tag{13}$$

For small voltages $V_{BB} << 2V_T$ the above equation simplifies to (12) and for large voltages $V_{BB} >> 2V_T$ (13) simplifies to (9). The boundary value of $2V_T$ was obtained with an assumption that the hole current is zero. This is not exactly true because holes are at the same time flowing and recombining along the device. The value $2V_T$ is not accurate and in a real device this boundary voltage can be expected to be much larger.

If it is assumed that the maximum injected hole concentration $p_{\max}$ is proportional to the emitter current I_E, then based on (13) the transistor characteristics can be described by

$$I_{BB} = \beta I_E\left[1 - \exp\left(-\frac{V_{BB}}{V_o}\right)\right] + \frac{V_{BB}}{R_H} \tag{14}$$

where R_H is the ohmic resistance between bases without hole injection, V_o is the boundary voltage, and β is the current gain coefficient.

The last two parameters could be different for positive or negative biasing. Fig. 17 shows measured device characteristics (solid line) and characteristics obtained using the transistor model given by (12) (dotted line) with the following parameters: $R_H = 4.1$ kΩ; $\beta = 4.0$; $V_o = 4.8$ V. Since a very simple model with three parameters was used, excellent agreement cannot be expected. For example, by inspecting Figs. 13 and 14 one may see that the space charge affects the current flow in the B region and therefore the phenomenon is not purely ohmic. The slight disagreement between measured and predicted current in the device is shown in Fig. 17 and may be attributed to the space-charge effects discussed above. This effect has not been incorporated into the simple device model presented herein. In the future a more accurate device model should be worked out.

For practical purposes transistor characteristics for both polarizations can be approximated by

$$I_{BB} = \beta I_E \tanh\left(\frac{V_{BB}}{V_o}\right) + \frac{V_{BB}}{R_H}. \tag{15}$$

This equation gives symmetrical characteristics for both polarities which is generally not true in a real device because in the case of negative polarization of base B_2 with respect to B_1 injected holes have a longer path to travel to reach the vicinity of the potential barrier. This longer path allows for recombination and the current gain β for this polarization is slightly lower.

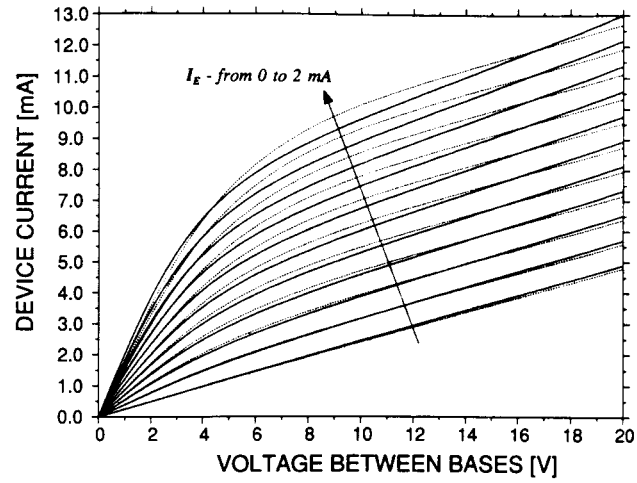

Fig. 17. Measured (solid curves) and calculated (dashed curves) CMT characteristics with calculations based on (20).

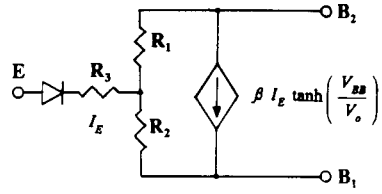

Fig. 18. An equivalent electrical circuit of the Conductivity Modulated Transistor.

An equivalent electrical circuit for the CMT is shown in Fig. 18. The sum of R_1 and R_2 represents R_H, the output resistance of this device. For positive polarization of B_2 higher input voltage is required to obtain the same input current. In the case of negative polarization, positive feedback can be observed which, in some cases with large R_1, may lead to negative input resistance and as a consequence to unstable operation. In order to minimize this undesired effect very careful device design should be carried out. The extra n-type region shorted to B_1, as shown in Fig. 1, is crucial for the design in order to obtain small R_1 and stable device operation. The design goal is to have $R_1 \Rightarrow 0$ and $R_2 \Rightarrow R_H$.

VI. Application

The conductivity-modulated transistors have very unique characteristics and can be used directly to control an ac circuit as shown in Fig. 19(a). The controlling circuit is a dc circuit with a current source. In the load circuit both dc and ac operations are possible, because the CMT transistor current between bases B_1 and B_2 is controlled by an emitter current, no matter in which direction the current flows, and is independent of the polarization voltage between B_1 and B_2.

It can be used in many ac-controlled circuits when large current distortion is not allowed (as in TRIAC or SCR

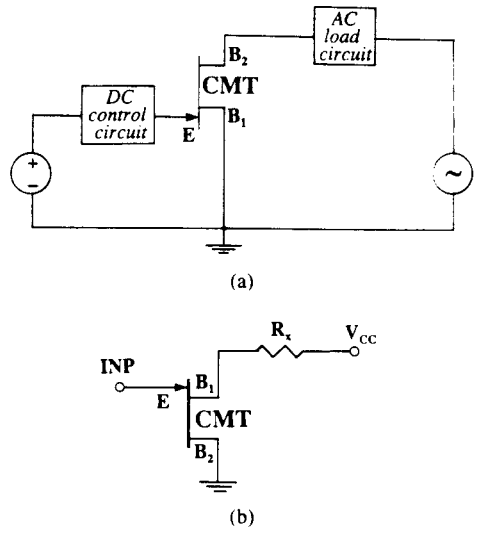

Fig. 19. Application circuits of Conductivity Modulated Transistor. (a) AC controlled circuit. (b) CMT as an equivalent of programmable unijunction transistor.

circuits). Also, when it is essential not to generate electromagnetic noise, the proposed CMT transistor can be very useful.

The device can be also used in applications where an electrically controlled resistor is required. Note that the device behaves as a resistor the value of which can be modulated by emitter current. The wide range of linear characteristics make this device particularly attractive in such applications.

It may also be used instead of conventional unijunction transistors which exhibit negative input resistance as is shown in Fig. 19(b). Similarly as in the Programmable Unijunction Transistor, various threshold voltages can be controlled by an external resistor R_x.

VII. Conclusion

In theory a very large β is possible when recombination phenomena are carefully controlled. However, high β values may create problems of unstable operation. Therefore, in order to assure a small value of R_1, careful design of the device geometry becomes critical.

The presented one-dimensional numerical analysis was helpful in understanding the physics of the device operation and allows for derivation of a simple analytical model. Better understanding of the device operation could be possible when two- or three-dimensional analysis is performed in the presence of hole current. This also may allow for the study of device geometry which may lead to the optimum device design with respect to lower values of R_1 for assurance of stable device operation. With the presented one-dimensional approach no such conclusion can be drawn.

Another possible approach is to fabricate many devices with various geometries and, based on the obtained characteristics, proper conclusions for optimum design can be drawn.

With silicon devices it will be difficult to obtain high ratios between the on and off states. In the measured device the ratio was about 4. It is, however, expected that in the case of GaAs, where much larger resistances are possible, this ratio can exceed 100.

References

[1] L. E. Clark, "Now new unijunction geometries," *Electronics*, vol. 38, pp. 93-97, 1965.
[2] T. Mimura, "Voltage-controlled DNR in unijunction transistor structure," *IEEE Trans. Electron Devices*, vol. ED-21, p. 604, 1974.
[3] Special Report: "The unijunction transistor," *Electronics*, vol. 38, no. 12, pp. 87-110, June 14, 1965.
[4] A. M. Taher, "Modeling the static emitter characteristics of unijunction transistors," *Int. J. Electron.*, vol. 66, pp. 597-599, Apr. 1989.
[5] N. A. Shyne, "Bipolar transistor pair simulates unijunction," *Electronics*, vol. 47, p. 113, Jan. 24, 1974.
[6] B. M. Wilamowski, Z. J. Staszak, and R. H. Mattson, "An electrical network approach to the analysis of semiconductor devices," to be published in the *IEEE Trans. Education*, vol. 35, pp. 144-152, May 1992.

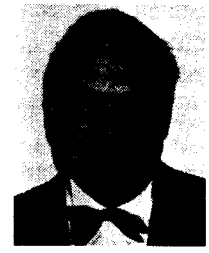

Bogdan M. Wilamowski (SM'83) received the M.S. degree in computer engineering in 1966, the Ph.D. degree in neural computing in 1970, and the D.Sc. degree in integrated circuit design in 1977, all from the Technical University of Gdańsk, Gdańsk, Poland.

He joined the faculty of the University of Gdańsk in 1966. He became Associate Professor in 1978 and Professor in 1987. During 1979-1981, he was the Director of the Institute of Electronic Technology and during 1988-1989, he was Head of the Solid State Electronic Chair there. From 1968 to 1970 he was with the Nishizawa Laboratory at Tohoku University, Japan, and he spent 1975-1976 at the Semiconductor Research Institute, Sendai, Japan, as JSPS Fellow. During 1981-1982, he was a faculty member at Auburn University, Auburn, AL, and during 1982-1984 he was a Visiting Professor at the University of Arizona at Tucson. Since 1989 he has been a Professor in the Electrical Engineering Department, University of Wyoming, Laramie. He is the author of 2 books, more than 100 publications, and about 30 patents in 7 countries. His main areas of interest are semiconductor devices, electronic and integrated circuits, computer simulation, and modeling.

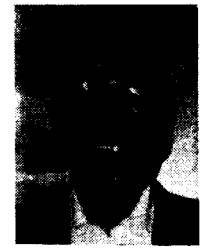

Thad J. Englert (M'85) received the B.S. degree in physics and mathematics in 1962 from the University of Northern Colorado, Greeley, the M.S. degree in physics from Iowa State University, Ames, and the Ph.D. degree in physics in 1983 from the University of Wyoming, Laramie.

He worked at the Iowa State Synchrotron Facility from 1964 to 1969, taught physics and mathematics at Colorado Mountain College, Glenwood Springs, from 1969 to 1976, and has been an Assistant Professor in Electrical Engineering at the University of Wyoming, since 1984. His research interests and publications have included interaction of laser radiation with matter, electrooptic effects in semiconductors, ionizing radiation effects on optical materials, and electrooptic sensing of high voltages. He is currently on leave at Phillips Laboratory at Kirtland AFB, NM.